Ballistic transport in InSb nanowires

Author	Affiliation	Email
Csonka, Szabolcs	BME	csonka.szabolcs@ttk.bme.hu
Geresdi, Attila	Chalmers	geresdi@chalmers.se
Sorba, Lucia	CNR	lucia.sorba@nano.cnr.it
Project Number	Project Start Date	Duration
828948	01.04.2019	48 Months
Classification		
	PU	
File Name		
WP No	Work Package Name	
1	Material developments	
Deliverable No	Deliverable Name	
D1.3	Ballistic transport in InSb nanowires as measured by quantized conductance plateaux	
	Approved by	
	Steering Committee of the action	

The opinions expressed in the document are of the authors only and no way reflect the European Commission's opinions. The European Union is not liable for any use that may be made of the information. This project has received funding from the European Union's Horizon 2020 research and innovation programme under grant agreement No 828948.

DOCUMENT REVISION HISTORY

Revision	Date	Description	Author
1.0			Szabolcs Csonka

Table of Contents

1. Introduction

Beside InAs, which is the major material platform of AndQC to realize qubits, InSb is a promising alternative, where the stronger spin-orbit coupling, the longer Fermi wavelength and the smaller band gap would provide advantages. The goal of the present deliverable is to establish InSb based platform in the consortium to realize Andreev bond states and later on Andreev qubits in multichannel weak links. InSb exists in nanowire form, however the Pisa node very recently had promising preliminary results with growing InSb nanoflags, which provides a more flexible structure to tailor the desired bound states. Thus, in the last period we put our effort in Task 1.1 of WP1 to investigate its applicability. This report summarizes our results on the growth, basic transport characterization, demonstration of ballistic transport and superconducting proximity.

2. Growth of InSb nanoflags

We have realized freestanding two-dimensional (2D) InSb nanoflags (NFs) large enough to be able to fabricate multiterminal devices. This was possible by carefully choosing a robust supportive stem, tapered InP nanowires (NWs), by aligning the samples with the help of the RHEED pattern, by optimizing the growth parameters, and by choosing the orientation of the stem in the direction that maximizes the NF elongation keeping the NF thickness at a minimum [1]. The resulting InSb NFs are (2.8 ± 0.2) µm long, (470 ± 80) nm in width, and (105 ± 20) nm of thickness, with defect-free zinc blende (ZB) crystal structure, stoichiometric composition, and relaxed lattice parameters, see Fig. 1.

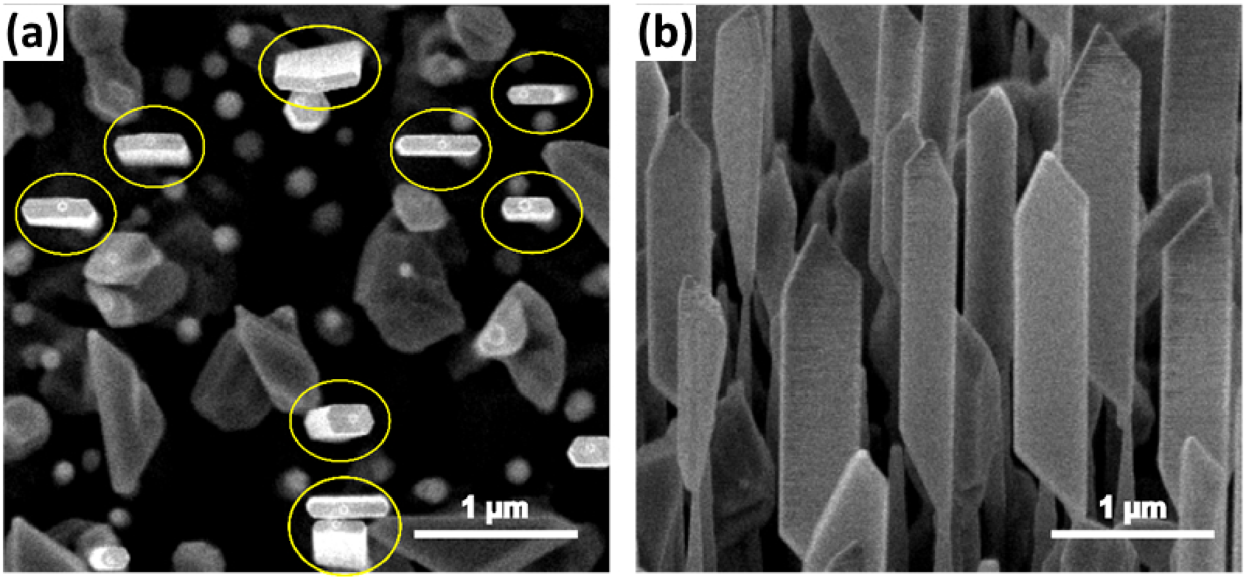

***Figure 1**: (a) Top view and (b) 45°-tilted SEM image of the InSb NFs (scale bar: 1 µm). The InSb NFs, which have a (width/thickness) ratio ≥ 4, are marked by yellow circles in panel a.*

3. Basic transport characterization

To investigate the electronic properties of the InSb NFs, we performed low-temperature (4.2 K) magnetoresistance measurements on Hall-bar devices (Fig. 2a). The presence of good Ohmic contacts with low resistance between the InSb NFs and the metal contacts and the absence of a Schottky barrier is confirmed by linear I_{SD}–V_{SD} curves. The variation of conductance as a function of back gate voltage was measured showing a charge carrier modulation with increasing positive back gate voltage, consistent with an n-type behavior of the InSb NFs. We performed a series of Hall-effect measurements at 4.2 K. The resulting charge-carrier densities and Hall-mobilities for various back-gate voltages are shown in Fig. 2b. Hall mobility increases with increasing back gate voltage and shows a maximum of about 29500 $cm^2/(V\ s)$ at $V_{BG} = 25$ V, with a corresponding electron density of $8.5 \times 10^{11}\ cm^{-2}$. Furthermore, we estimated the electron mean free path λ_e, using $\lambda_e = (\hbar\mu/e)(2\pi n)^{1/2}$, with $\hbar$ the reduced Planck's constant and n the 2D electron density from the Hall measurements. As shown in Fig. 2c, λ_e reaches values of ~500 nm for $V_{BG} \geq 25$ V, which compares favorably with literature.

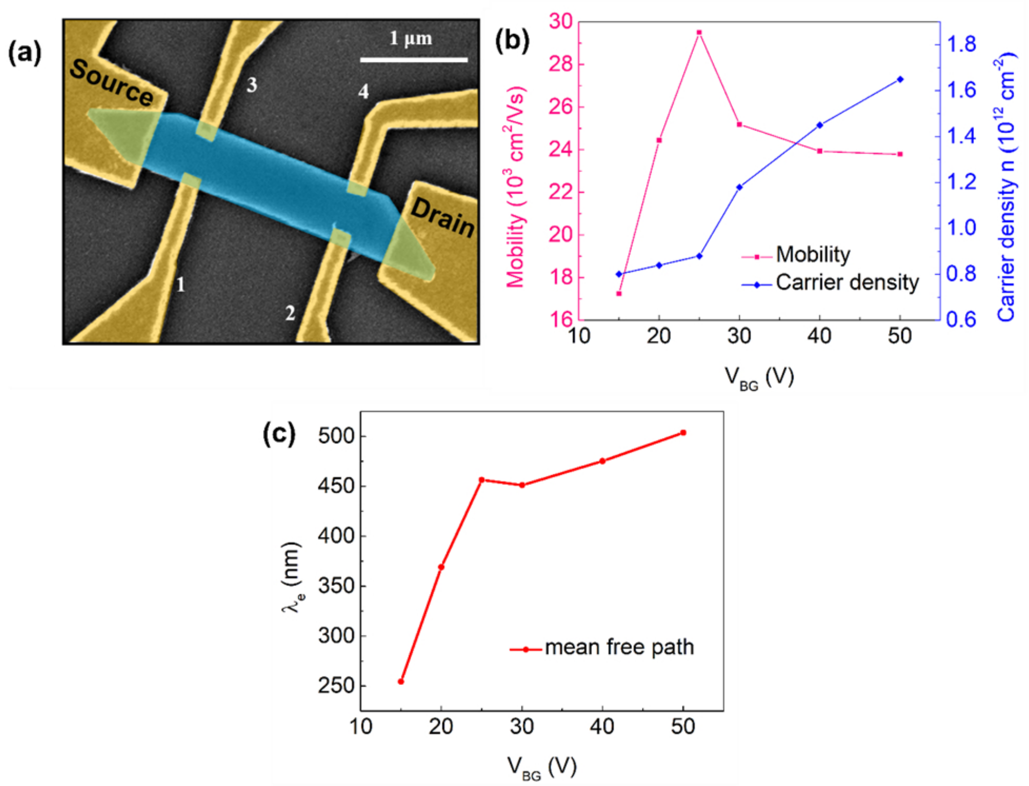

***Figure 2**: (a) SEM image of an InSb NF Hall-bar device with corresponding numbers for Hall-bar contacts. (b) Mobility and charge carrier density obtained from Hall measurements. (c) Elastic mean free path λ_e as a function of back gate voltage V_{BG}. All measurements are performed at a temperature of 4.2 K.*

4. Ballistic nanowires etched from InSb nanoflags

Below, we demonstrate that the few propagating channel regime with high transparency can reproducibly be realized using the InSb nanoflag platform.

We started the device fabrication by creating backgate structures on an intrinsic Si wafer. These bottom gates consist of a metallic layer of Ti/Au covered by a nominally 20 nm thick AlO_x insulator created by atomic layer deposition (ALD). We then deterministically deposited the InSb nanoflags from the growth chip on the bottom gates by a micromanipulator under an optical microscope. Next, we selectively etched the nanoflag with a 1:10 solution of $(NH_4)_2S_x$ in water at the areas defined by standard positive tone electron beam lithography. We confirmed that the nanoflag was completely etched through in 4 minutes at 40 C. After this step, we defined the Ohmic contacts to the nanoflag, the side gates and the contacts to the bottom gates and deposited a Ti/Au bilayer (5nm/180 nm) after a milder wet etching with a 1:20 solution of $(NH_4)_2S_x$ in water at 35 C for one and half minutes. The electrical measurements were performed in a dilution refrigerator at a temperature of approximately 30 mK in a magnetic field perpendicular to the substrate. Conductance measurements were performed by a standard low-frequency lock-in technique with an excitation voltage of the order of $10\mu V$. The two devices discussed in this report are shown in Fig. 3a and b.

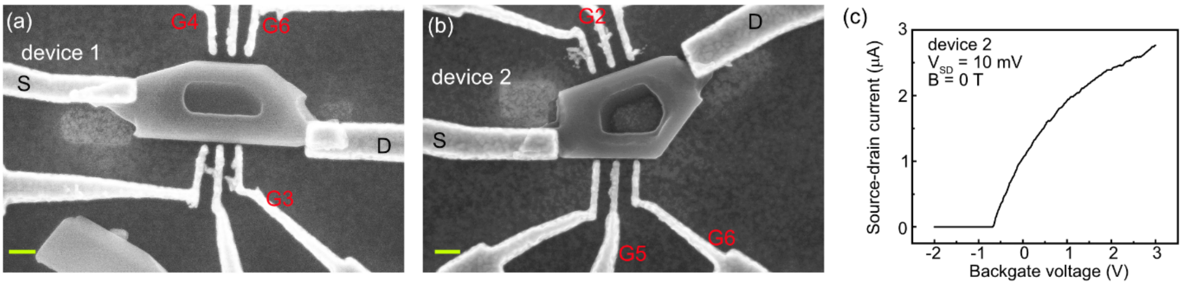

***Figure 3**: Panels (a) and (b) show SEM images of the two InSb nanoflag devices discussed in this report. Note that due to electrical shorts between adjacent leads and because of some open connections, not all of the side gates were operational. The working sidegate designations are overlaid in red, and the Ohmic leads are labelled as S (source) and D (drain), respectively. The yellow scale bar denotes 200 nm. (c) Backgate pinchoff trace of device 2, demonstrating a saturation resistance less than approximately 3 kΩ.*

We first characterized the response of the device to the backgate voltage, which simultaneously changes the charge carrier density in both arms and the contact areas. An example curve is shown in Fig. 3c, demonstrating a saturation current in excess of 3 µA at a source-drain voltage bias of 10 mV, which is in correspondence with earlier transport measurements on similar devices [1]. Next, we investigated individual side gate control (Fig. 4a) demonstrating the tuning of each arm of the device with their respective side gates. Note that for device 1, we scanned G4 and G6 together, and used the same procedure in the case of G5 and G6 for device 2.

Operating device 1 in a regime where the lower arm (see Fig. 3a) is depleted, we found quantized conductance plateaus as shown in Fig. 4b, which develop in finite magnetic fields, where a spin-polarized plateau at $G = 0.5 \times 2e^2/h$ emerges. The height of this plateau on the source-drain bias voltage axis equals to the Zeeman splitting of the lowest subband, $eV_{SD} = E_Z = g\mu_B B$, where B is the applied magnetic field, g is the Lande g-factor and μ_B is the Bohr magnetron (Fig. 4c). A linear fit to the plateau height as a function of the magnetic field (inset of Fig. 4c) yields $g = 34.2$, consistent with prior experiments on the same material. These results together prove that nanowire-like structures etched of InSb nanoflags can host conducting channels of high transmission, and can be tuned into the single subband regime, as required for the individually manipulation of Andreev bound states.

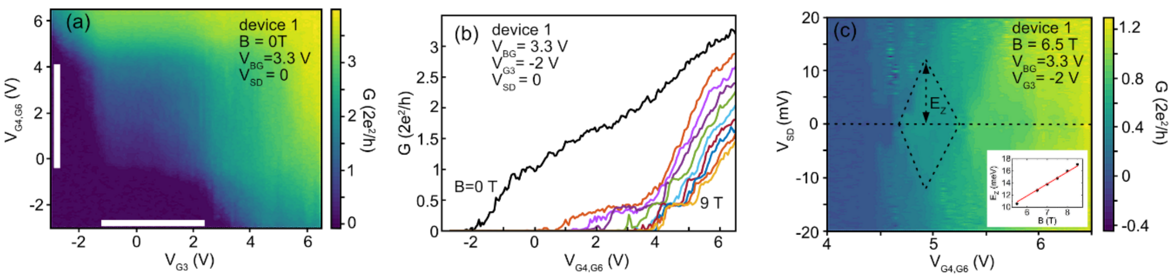

***Figure 4**: (a) Individual side gate control of the zero-bias conductance, G on device 1. Independent pinch-off of each arm is achieved in the side gate voltage range denoted by the white bars. However, because of gate drift, we used slightly more negative V_{G3} values in subsequent measurements. (b) Quantized zero bias conductance in the upper arm of device 1 with the lower arm fully depleted. Line traces are taken at magnetic fields incremented by 1 T between 0 and 9 T. (c) Measurement of the height of the $0.5 \times 2e^2/h$ plateau on the source-drain bias voltage axis. The inset shows the plateau height as a function of the magnetic field and the linear fit yields a Lande g-factor of $g = 34.2$ for the lowest subband.*

To demonstrate the reproducibility of the above results, we performed similar measurements on device 2. Fig. 5a and b showcase the emergence of the lowest spin-polarized quantized conductance plateau when only one of the arms is open. Finally, we demonstrate phase-coherent transport through the device by characterizing the conductance fluctuations as the function of the applied perpendicular magnetic field while both arms are open (Fig. 5c). Here, the expected periodicity of the Aharonov-Bohm effect is $\Delta B = \Phi_0/A$, where $\Phi_0 = h/e$ is the flux quantum and A is the cross-sectional area of the device. We note that because of the relatively wide arms surrounding the central hole, we expect no well-defined oscillation period, however typical values of $\Delta B = 20\ to\ 40$ mT are consistent with the device geometry, thus proving that electronic transport is phase coherent through the loop. Future devices with higher aspect ratio (thinner arms) should yield better defined oscillation periodicity.

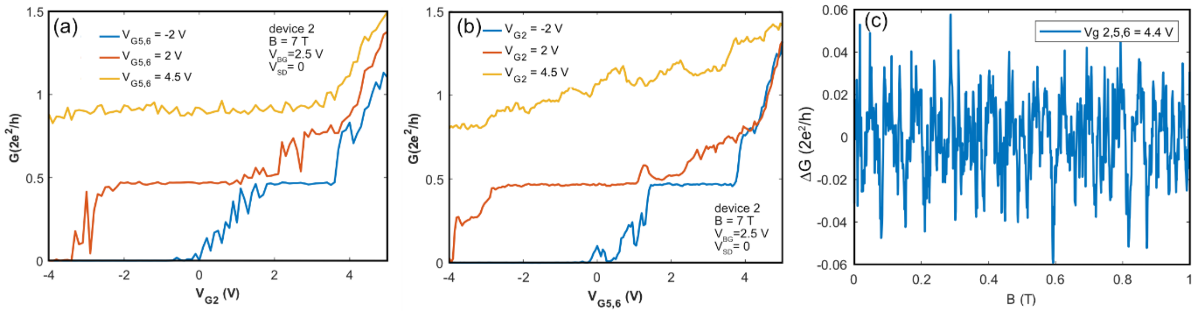

Figure 5: *Panels (a) and (b) demonstrate quantized conductance plateaus measured on device 2 in its upper and lower arm, respectively, while the other arm is fully depleted. (c) Conductance oscillations on the same device demonstrate phase coherent transport. The typical 20 to 40 mT oscillation periodicity is consistent with the surface area of the loop (see Fig. 3b). Note that the smooth background of* $G \approx 2e^2/h$ *was subtracted from the raw experimental data.*

5. Transport in ballistic InSb nanoflag Josephson junctions

We also fabricated and characterized Josephson junction (JJ) devices based on these InSb NFs and provide evidence of ballistic superconductivity. For the first time, we employed Ti/Nb contacts in InSb JJ devices. The devices show gate-tunable proximity induced supercurrent at 250 mK and clear signatures of subharmonic gap structures, indicating phase-coherent transport in the junction and highly transparent interfaces [2]. Our results indicate InSb nanoflags as a promising platform for the study of Andreev bound states.

The upper left inset of Fig. 6 shows a SEM image of a JJ device. A 100 nm-thick InSb NF was transferred mechanically on a SiO_2/Si substrate and contacted with 10/150 nm Ti/Nb. The interelectrode spacing between the two superconductors, i.e., the length of the normal (N) region, is L = 200 nm, while its width is W = 700 nm. Standard transport characterization (see Fig. 2c) yields a mean-free path of $\lambda_e \sim 500$ nm [1] for the N region, greater than the junction length L. These numbers place the device in the ballistic regime.

Fig. 6 shows a typical $V - I$ curve obtained at T = 250 mK and V_{bg} = 30 V. The device displays well-developed dissipationless transport thus demonstrating proximity-induced superconductivity in the InSb NFs. As the bias current exceeds the critical value of $\sim$50 nA, a sudden jump in the measured voltage to a dissipative quasiparticle branch is observed, indicating that the Josephson junction switches from the superconducting to the normal state, with a resistance of $\sim$330 Ω.

The lower right inset to Fig. 6 shows the differential resistance *dV/dI* measured using a lock-in amplifier together with the $V - I$ curve. Data clearly show that the differential resistance is zero in the supercurrent branch of the device.

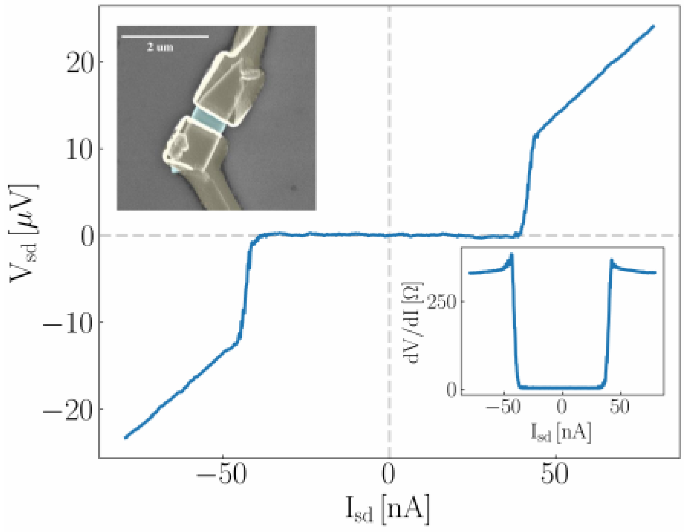

Figure 6: *Voltage drop V_{sd} as a function of bias current I_{sd}. A supercurrent of ~ 50 nA is observed. The lower right inset shows the differential resistance dV/dI measured simultaneously. V_{bg} = 30 V, T = 250 mK. The upper left inset shows a SEM image of the device structure. Scale bar 2 µm.*

6. Conclusion

In conclusion, we have introduced the growth of high quality InSb nanoflags with long mean free path. We have shown the creation of quasi-one dimensional channels, where a few electronic modes propagate with high transparency, as needed for the scientific goals of AndQC. We have also reported that superconducting proximity can be introduced in the nanoflags. With these results, we have demonstrated that InSb nanoflags are viable alternatives to InSb nanowires with similar Lande g-factor values. The nanoflag platform however has the added advantage of larger contact areas as well as the fabrication of more versatile devices at will.

References

[1] I. Verma, S. Salimian, V. Zannier, S. Heun, F. Rossi, D. Ercolani, F. Beltram, and L. Sorba, ACS Appl. Nano Mater. 4, 5825 (2021).

[2] S. Salimian, M. Carrega, I. Verma, V. Zannier, M. P. Nowak, F. Beltram, L. Sorba and S. Heun, submitted (2021).